ADVANCED ENGINEERING MATERIALS

DOI: 10.1002/adem.201500532

Direct Deposit of Highly Reactive $Bi(IO_3)_3$- Polyvinylidene Fluoride Biocidal Energetic Composite and its Reactive Properties**

By *Xiuli Hu,† Jeffery B. DeLisio, Xiangyu Li, Wenbo Zhou* and *Michael R. Zachariah**

Metal iodate oxidizers are synthesized and evaluated as oxidizers in thermite reactions to generate both heat and a biocidal reaction product for bioagent defeat. TGA/DSC/MS and T-jump TOFMS analysis show gas-phase iodine release from metal iodate decomposition at both low and high heating rates. In constant volume combustion tests, $Bi(IO_3)_3$/Al thermite outperforms other metal iodate/Al and traditional thermites. Mechanically sound composites with high mass loadings of particulates are formed by direct electrospray of synthesized metal iodates, nanoaluminum fuel, and polyvinylidine fluoride (PVDF) binder/oxidizer, and burn speeds are measured in both air and argon atmospheres.

1. Introduction

In response to the threat of bioterrorism, new methods for inactivation and neutralization of spores and bacteria are being explored.[1–3] Conventional neutralization nominally involves rapid delivery of thermal energy and high pressures, but the transient nature of the event may still result in insufficient neutralization efficiency. This has spurred the development of multifunctional reactive materials with biocidal combustion products, which remain active for an extended period of time well past the thermal and pressure pulse. Because of the desire to minimize over-pressures that can serve to disperse biological agents, consideration has been given to metalized systems that have high energy density with a lowergas release. These nominally can be classified as thermites systems.[4–8] Various methods to inactivate bioagents have been explored. The groups of Dreizin et al and Grinshpun et al have collaboratively prepared composites of Al–I_2 using mechanical milling, and have explored both the combustion and biocidal effectiveness resulting from both the thermal event and iodine release (the biocide).[9–12] Pantoya and co-workers[2,13] has considered Al combined with both I_2O_5 and silver oxide. Our group investigated a thermite consisting of Al and $AgIO_3$, which was shown to outperform CuO and Fe_2O_3-based thermites in pressure cell tests.[14,15] Further work by us using Ag_2O which has a high silver content was found to be relatively unreactive.[16] None of these materials has thus far been found to be the final solution. For example, Al–I_2 is unstable over long periods, I_2O_5 is moisture sensitive, Al and Ag_2O does not vaporize silver, and iodine was not released during the reaction between Al and $AgIO_3$.[10,12,13,15,17] Probably the most biocidally active energetic material for the forcible future will be based on iodine systems. Iodine effectiveness comes from interactions with the thiol groups in enzymes and proteins, iodination of phenolic and imidazole groups of tyrosine and histidine, and lipid interactions in lipid-enveloped viruses and phospholipids in bacteria.[18,19] Ideally, one would like a material which is stable during storage, easy to handle, containing a high mass fraction of iodine, undergoes a highly exothermic redox reaction with aluminum, and release molecular iodine.

Metal iodates offer many of the advantages outlined above, with iodine content up to 67.9% for the metal iodates listed in Table 1. The basic reaction stoichiometry of a generic metal iodate is shown in Equation 1. In the case of $AgIO_3$ however, the silver reacts with the iodine to form AgI, which while known as a biocide, is less effective than either Ag or I_2.[15] Nevertheless, there are many other metal iodates to choose from. In previous studies, we have used metal iodates

[*] *Prof. M. R. Zachariah, Dr. X. Hu, J. B. DeLisio, Dr. X. Li, Dr. W. Zhou*
Department of Chemical and Biomolecular Engineering and Department of Chemistry and Biochemistry, University of Maryland, College Park, Maryland 20742, United States
E-mail: mrz@umd.edu

[†] *Permanent address: School of Chemical Engineering, Nanjing University of Science and Technology, Nanjing, Jiangsu 210094, China*

[**] *This work was carried out with the support of the Defense Threat Reduction Agency. Xiuli Hu is grateful for the financial support from China Scholarship Council. (Supporting Information is available online from Wiley Online Library or from the author).*

Table 1. Combustion cell results of thermites samples prepared with different oxidizers. Thermites samples were prepared at stoichiometric ratio.

Oxidizers [w/Al, $\varphi = 1$]	Theoretical iodine content [wt%]	Burn time [μs]	P_{max} [MPa]	Pressurization rate [GPa s^{-1}]
$Bi(IO_3)_3$	51.9	144.9	1.9	1 260
$Fe(IO_3)_3$	65.6	845	0.2	0.2
$Ti(IO_3)_4$	67.9	378	0.28	0.0003
$AgIO_3$[15]	44.9	172	0.3	57
Nano-Fe_2O_3[14]	0	936	0.09	0.12
Nano-CuO[14]	0	192	0.8	61.5

Note: φ here is calculated based on $\varphi = \frac{\left(\frac{F}{O}\right)_{ACT}}{\left(\frac{F}{O}\right)_{ST}}$.

assembled in the form of microparticles comprising nano-aluminum and a gas generator to facilitate the reaction.[20] Metal iodates-based thermites show significantly improved reactivity and sporicidal performance over conventional metal oxide-based thermites.

$$2x\ \mathrm{Al} + \mathrm{M(IO_3)}_x \rightarrow x\ \mathrm{Al_2O_3} + \frac{x}{2}\mathrm{I_2} + \mathrm{M} + \Delta H \quad (1)$$

For the biocidal energetic applications, there are advantages to employing a composite that goes beyond the loose powder system typically employed. In this case, we build on our prior work on 3D printing of propellants.[21] In addition, a film structure is ideal for evaluation of mechanical and combustion properties due to a well-defined geometry and architecture.[22–24] One generic problem in any film formulation based on casting is that high loading of nanoparticles are difficult to achieve due to the rapid increase in viscosity of the mixture. This can also lead to an aggregation, inhomogeneous mixture, and poor mechanical properties.[25,26] The direct write employed here that uses the electrospray approach offer advantages in mitigating the high loading constraints.

Various binders have been used, including epoxy, nitrocellulose, paraffin, and various fluoropolymers, such as Viton fluoroelastomer (Viton)[27] and PVDF.[24] Fluorine is the most electronegative element, making it a candidate as an oxidizer in a redox reaction,[28] because the heat of reaction of Al/Teflon is much higher than that of best molecular explosive.[29] Unfortunately, because of its poor solubility, Teflon is not widely used in energetic formulations, although the content of fluorine in the polymer is high. Alternatively, we may consider PVDF, which has much improved solubility in organic solvents, with good mechanical properties similar to Teflon, albeit with a lower fluorine content.

In this paper, we focus on developing a composite film containing metal iodates, nanoaluminum, and a reactive polymer by a direct deposition method (Electro-spray or electrohydrodynamic deposition). This approach enables the eventual ability to make graded and laminate structure as we have described previously,[21,30] at high particle loadings. Several metal iodates were synthesized before the choice of $Bi(IO_3)_3$ was finalized on, based on its superior combustion performance. PVDF was chosen as the binder in the films which were deposited using electrospray, and were characterized for decomposition, combustion, and mechanical properties.

2. Experimental Sections

2.1. Materials

The aluminum nanopowders (Al-NPs) (Alex, 85 nm) used in this work was purchased from Novacentrix. The active Al was 81% by mass, determined by TGA. PVDF (Average M_w 534000 by GPC), N, -N, -Dimethylformamide (DMF) (99.8 wt%), and Ammonium perchlorate (AP) (99.8 wt%), Iodic acid (HIO_3) (99.5 wt%) purchased from Sigma–Aldrich was directly used as received. All the other chemicals were of analytical grade and used as purchased without further treatment. Bismuth iodate, iron iodate, silver iodate, and titanium iodate were synthesized using wet chemistry methods.

2.2. Synthesis of Metal Iodates

Bismuth iodate nanopowders were synthesized from 460 mg $Bi(NO_3)_3 \bullet 5H_2O$ dissolved into 10 mL DI water, to which was added 7.8 mol L^{-1} HNO_3. The solution was stirred approximate 10 min until it became clear. 500 mg HIO_3 was dissolved into 20 mL DI water. The HIO_3 solution was then added to the $Bi(NO_3)_3$ solution under vigorous stirring. As the HIO_3 solution was added, a white precipitate immediately formed which was subsequently collected by vacuum filtration. The product was washed four times using DI water, dried in the fume hood for 12 h, and then grounded into a fine powder. (The procedures and properties of iron iodate and titanium iodate can be found in supporting materials).

2.3. Preparation of Precursors

The synthesized bismuth iodate ($Bi(IO_3)_3$) nanoparticles were dispersed with 30 min sonication in DMF, and then Al-NPs was gently added, followed by another 30 min ultrasonication. In our previous work, we find that a small quantity of AP in the precursor can significantly improve the morphology and mechanical property of the films.[21] In a typical experiment, 141.2 mg of $Bi(IO_3)_3$ nanoparticles, 107.9 mg Al-NPs, 200 mg PVDF, and 4.5 mg AP was dissolved in 4 mL DMF. The suspension obtained above was sonicated for another 30 min, and then magnetically stirred for 24 h before use.

2.4. Film Deposition

As presented in Figure 2A, films were deposited using electrospray methods previous used by our group.[21,30] In this work, the precursor was fed at a fixed rate of 2 mL h^{-1} with a syringe pump, through a flat-tip stainless needle with a 0.43 mm inner diameter under a working voltage of 18 kV. The jet-to-substrate distance was kept at 4.5 cm to provide

DOI: 10.1002/adem.201500532

sufficient time for some solvent evaporation, although the deposition is conducted wet. The thickness of the films could be easily adjusted by changing the duration of electrospray deposition. The experimental apparatus was shielded in an insulated box to reduce the possible dangers posed by high voltage and spark ignition.

2.5. Characterization

2.5.1. X-Ray Diffraction

Bismuth iodate and the post-combustion products were characterized by powder X-ray diffraction (XRD; Bruker C2 Discover with GADDS, operating at 40 kV and 40 mA with unfiltered Cu Ka radiation, E¼8049 eV, k¼1.5406 Å).

2.5.2. Electron Microscopy

The morphology of bismuth iodate was determined by transmission electron microscopy (TEM, JEM 2011 LaB6 TEM), while the thickness of the films were characterized by a scanning electron microscopy (SEM, Hitachi, Su70 FEG-SEM). For the cross-sectional images, the samples were first fractured in liquid nitrogen and then cleaved.

2.5.3. TGA

TGA and Differential Scanning Calorimetry (DSC) were conducted using a SDT Q600 (TA instruments) equipped with a TA Discovery MKS104-S0212004 Micro Vision 2 mass spectrometer. The analysis was performed under a 50 mL min^{-1} nitrogen flow with 0.9–1.0 mg samples placed into an alumina pan and heated from room temperature up to 800 °C at a rate of 10 °C min^{-1} in argon atmosphere.

2.5.4. Combustion Evaluation of Powders

Combustion properties of powders were evaluated in a constant-volume combustion cell, with simultaneous pressure and optical emission measurements. In a typical experiment, 25 mg of thermite powder was loaded in the cell (constant volume, ≈13 cm^3) and ignited by a resistive heated nichrome wire. The pressurization rate was expressed as the peak pressure (KPa) divided by the pressure rise time (μs). The characteristic burn time of thermite is represented by the full-width at half-maximum (FWHM) of the recorded optical signal intensity. More detailed information of the combustion cell test can be found in our prior publications.[31]

2.5.5. Temperature Jump Time of Flight Mass Spectrometry (T-Jump TOFMS)

T-jump TOFMS was performed using the previously described home-built instrument.[32–34] Powder samples were suspended in hexane and deposited manually via micropipette, and film samples were electrosprayed, onto a 70 μm diameter platinum wire for the TOFMS and ignition temperature test, respectively. The heating rate of the platinum wire was approximately 5×10^5 K s^{-1} in these experiments for about 3 ms. A sampling rate of 100 μs per spectrum (10 kHz) was used to capture the progress of the reaction with 95 spectra obtained post-triggering for each run. The data were sampled using 500 MHz digital oscilloscope and transferred to a PC for further analysis. The details of T-Jump mass spectrometry can be found in our previous publications.[35]

2.5.6. Mechanical Properties

The mechanical properties of as-prepared $Bi(IO_3)_3$/Al/PVDF films were tested by a custom-built microtensile tester. Specimens with gauge length of 2.5 cm and width of 0.5 cm were attached to the stages. For every film, three specimens were tested at a quasistatic loading strain rate of 10^4 s^{-1} controlled by customized picomotor control software. A video extensometer comprising of a Point Grey Flea 2 (FL2-14S3C) digital camera and a stereo microscope was used for the acquisition of the specimen strain in the gauge section.[36,37] The stress is calculated by the ratio of force measurement from the load cell to the initial measurement thickness and width of the sample gauge section.

2.5.7. Propagation Velocity of Films

The combustion properties of the films were captured by a high-speed camera (Phantom v 12.0) with a frame rate of 7 000 frames per second in both air and argon environments. Typically, a 3×0.5 cm^2 film was fixed between a nichrome wire igniter and a holder (shown in supporting material Figure S1) in an atmosphere-controlled combustion chamber. The combustion of $Bi(IO_3)_3$/Al/PVDF films were conducted under an argon or air atmosphere, and evaluated in triplicate for each sample condition to determine propagation velocity. Following combustion, the condensed residue was collected for XRD evaluation.

3. Results and Discussion

3.1. Combustion Properties of Metal Iodate/Al Thermite

Various metal iodate-based energetic formulations were prepared by mixing $Bi(IO_3)_3$, $Fe(IO_3)_3$, and $Ti(IO_3)_4$, with Al-NPs in a stoichiometric ratio respectively, as shown in Equation 1. The relative reactivity of metal iodate-based thermite was evaluated using a constant volume combustion cell (Figure S2A) to obtain temporal pressure and optical emission profiles as shown in Figure S3. The iodine content, full-width at half-maximum burn time, peak pressure, and pressurization rate are tabulated in Table 1, for $Bi(IO_3)_3$, $Fe(IO_3)_3$, $Ti(IO_3)_4$, with $AgIO_3$, Fe_2O_3, and CuO as reference materials.

As shown in Table 1 and Figure S3A, the pressure profile of $Al/Bi(IO_3)_3$ shows a rapid rise, which occurs in less than a microsecond, with peak pressure ≈2 MPa, and average pressurization rate is up to ~1 260 Gpa s^{-1} (Table 1). Both the maximum pressure and the pressurization rate of $Al/Bi(IO_3)_3$ thermite significantly outperform $Al/Fe(IO_3)_3$, $Al/Ti(IO_3)_4$, $Al/AgIO_3$, Al/nano-Fe_2O_3, Al/nano-CuO (Table 1 and Figure S3). The normalized optical emission trace of $Al/Bi(IO_3)_3$ shows that the burn time is ≈145 μs, which is much longer than the

pressure-rise time, suggesting that burning is rate limited by the aluminum, since the pressure rise is primarily attributed to the decomposition of the oxidizer releasing oxygen.[38,39] These results point to $Al/Bi(IO_3)_3$ thermite as the best performing iodate, which leads us to focus the remainder of the paper on $Bi(IO_3)_3$-based systems.

3.2. Decomposition of Bismuth Iodate

The superior behavior of $Al/Bi(IO_3)_3$ in the combustion cell test indicates that substantial gas is released during the redox reaction, which can be correlated to the thermal decomposition features of $Bi(IO_3)_3$. Therefore, in this section, we evaluate the decomposition behavior of the synthesized $Bi(IO_3)_3$ at both low and high heating rates.

3.2.1. Decomposition at Low Heating Rate ($10\,K\,min^{-1}$)

Figure 1A shows that the synthesized $Bi(IO_3)_3$ particles while agglomerated, are relatively spherical with an average diameter size of ≈90 nm. TGA and DSC of $Bi(IO_3)_3$, in conjunction with I_2^+ and O_2^+ mass spectrum intensities are shown in Figure 1B and C. Using this combined data the decomposition steps, reactions, and weight loss of $Bi(IO_3)_3$ are tabulated in Table 2.

The DSC indicates an endotherm at about 125 °C (step a), which we attribute to the evaporation of H_2O. The two exotherms at 300 °C (step b) and 375 °C (step c), we believe correspond to an amorphous to crystalline phase transition (see XRD patterns in supporting materials Figure S4A and B) and a second phase transition at 375 °C (Figure S4B and C, both of which occur with no mass change detected in the TGA.

We explain the decomposition of $Bi(IO_3)_3$ from TGA/DSC/MS as occurring in three steps (d, e, and f) (Figure 1B) and summarized in Table 2. Following heating, $Bi(IO_3)_3$ decomposition yields Bi_2O_3 as a residue.[40] The first step is initiated with a small endotherm with a 3.4% mass decrease at about 410 °C, which can be indexed to the equation displayed in step d, and the appearance of O_2^+ in the mass spectrum. This is followed by an endotherm at about 530 °C, with a 39.1% mass loss. In this step, both O_2^+, and I_2^+ are observed corresponding to the reaction in step e and Figure 1C. The third sharp endotherm losses another 23.6% weight at roughly 560 °C (step f) can be seen in Figure 1B and Table 2. The last decomposition step gives Bi_2O_3 as a residue, with O_2, and I_2 loss. From 570 to 750 °C (step j), there is an additional 3.2% weight loss which remains unexplained. We can deduce the heat of formation of $Bi(IO_3)_3$ from the following Equation 2 (combing equations in steps d–f):

$$Bi(IO_3)_3 \rightarrow \frac{3}{2}I_2 + \frac{15}{4}O_2 + \frac{1}{2}Bi_2O_3 \qquad (2)$$

$\Delta H_{dec} Bi(IO_3)_3 = -466.8\,kJ\,mol^{-1}$ was calculated from DSC results in Figure 1B and the $\Delta H_f\, Bi_2O_3 = -573.2\,kJ\,mol^{-1}$ was obtained from ref.[41] We obtain a value of: $\Delta H_f\, Bi(IO_3)_3 = -753.4\,kJ\,mol^{-1}$

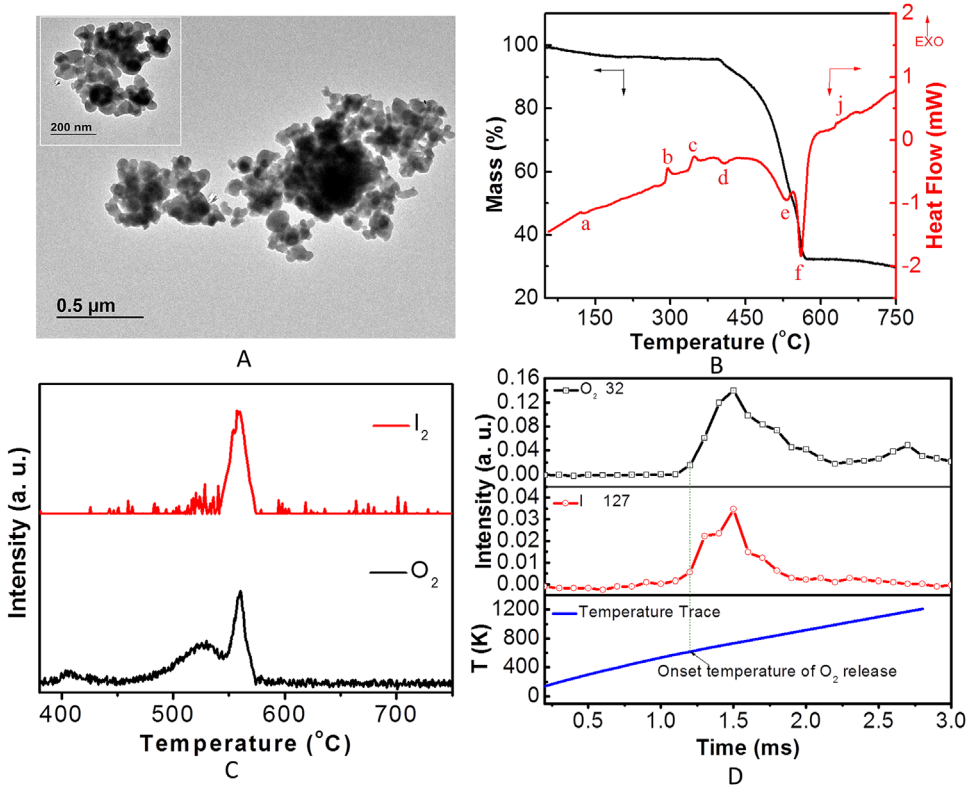

Fig. 1. TEM image of synthesized $Bi(IO_3)_3$ (A); TGA and DSC curves of $Bi(IO_3)_3$ (B) with O_2^+, and I_2^+ mass spectrum intensities (C); transient gas release profiles and temperature trace determined by rapidly heating $Bi(IO_3)_3$ in the T-jump mass spectrometer (D).

DOI: 10.1002/adem.201500532

Table 2. Decomposition steps of $Bi(IO_3)_3$ under low heating rate (10 K min^{-1})

Steps	Temperature range [°C]	Physiochemical changes	Theoretical weight loss for reaction [%]	Experimental △H [kJ kg^{-1}]	Observed weight loss [%]
A	50–300	Evaporation of bound H_2O	–	−2.6	3.6
B	300	Crystallization	0	15.9	0
C	375	Phase change	0	14.5	0
D	375–410	$Bi(IO_3)_3 \rightarrow Bi(IO_2)_3 + \frac{3}{2}O_2 + \Delta H$	6.5	−636.0 (overlapped)	3.4
E	410–535	$Bi(IO_2)_3 \rightarrow BiIO_4 + O_2 + I_2 + \Delta H$	38.9		39.1
F	535–570	$BiIO_4 \rightarrow \frac{1}{2}Bi_2O_3 + \frac{5}{4}O_2 + \frac{1}{2}I_2 + \Delta H$	22.8		23.6
J	570–750	Unidentified	–	16.5	3.2

3.2.2. Decomposition of Bismuth Iodate at High Heating Rate ($\approx 5 \times 10^5$ K s^{-1})

T-jump/TOFMS was also employed to observe the decomposition of $Bi(IO_3)_3$ particles under high heating rate ($\approx 5 \times 10^5$ K s^{-1}) as shown in Figure S2B, with mass spectra obtained at 10 kHz, enabling one complete spectra every 100 μs. Under rapid heating ($\approx 5 \times 10^5$ K s^{-1}), the decomposition of $Bi(IO_3)_3$ differs from that observed at the much slower heating rate (10 K min^{-1}) TGA/DSC test, and can be divided into only two steps according to the time-resolved mass spectra shown in Figure 1D. The initial step has an onset temperature of 620 °C (Figure 1D), which is much higher than that in the TGA/DSC result (410 °C in Figure 1B) due to the employment of a much higher heating rate ($\approx 5 \times 10^5$ K s^{-1} vs. 10 K min^{-1}). The full time-resolved mass spectra of $Bi(IO_3)_3$ decomposition under rapid heating is shown in Figure S5. Early on (730 °C, $t = 1.5$ ms), decomposition products include O_2^+, IO^+, IO_2^+, and I_2^+. During the second step, in addition to O_2 and I_2, Bi^+ and BiO^+ are also observed. According to the results of TGA/DSC and T-jump/TOFMS, the decomposition of $Bi(IO_3)_3$ under both low and high heating rate release iodine.

3.3. Reaction of Al/$Bi(IO_3)_3$ Thermite at High Heating Rate ($\approx 5 \times 10^5$ K s^{-1})

In order to further study the combustion property of Al/$Bi(IO_3)_3$ thermite, T-jump/TOFMS was conducted to observe the ignition and combustion of Al/$Bi(IO_3)_3$. We find an ignition temperature of Al/$Bi(IO_3)_3$ of ≈650 °C ($t = 1.60$ ms) as optically observed by the high-speed camera (selected frames of Al/$Bi(IO_3)_3$ combustion in vacuum (Figure S6A). The ignition (≈650 °C) occurs after the point of gas phase release of O_2 from pure $Bi(IO_3)_3$ (≈620 °C) and essentially at the temperature around the melting point of Al-NPs (≈660 °C). O_2^+, I^+, and I_2^+ were also observed as shown in Figure S7, which was consistent with the decomposition of pure $Bi(IO_3)_3$, and showing that the Al/$Bi(IO_3)_3$ reaction also releases iodine.

3.4. $Bi(IO_3)_3$/Al/PVDF Composite Films

Our previous research[21] showed that Al/ PVDF could be fabricated in a direct write mode to create 3D printed propellant. In this study, we have so far shown that $Bi(IO_3)_3$ when reacting with Al can generate both heat and biocidal iodine. Next we incorporate this ingredient into an energetic $Bi(IO_3)_3$/Al/PVDF biocidal film.

3.4.1. Physical Characteristics

$Bi(IO_3)_3$/Al/PVDF films were deposited using an electrospray method as shown in Figure 2A and described in our prior work.[5,30] In these films, both PVDF and $Bi(IO_3)_3$ are oxidizers, and the mass loadings are based on Equation 3 and 4. For example, for $m_{(PVDF:Al-1):}m_{Bi(IO_3)_3/Al-2)}$ of 80:20, the mass of reactants in Equation 3 is 80%, while that in Equation 4 is 20%. This is designated as an F20 film. All of the films were prepared in this manner to have a zero oxygen balance. We also calculate the total mass% of particulate phase in the film, as the sum of aluminum and bismuth iodate relative to PVDF. These parameters are shown in Table 3.

$$3(CH_2 - CF_2)_n + 2n\mathrm{Al} - 6n\mathrm{C} + 2n\mathrm{AlF_3} + 3n\mathrm{H_2} \quad (3)$$

$$Bi(IO_3)_3 + 6\mathrm{Al} - \mathrm{Bi} + 1.5\mathrm{I_2} + 3\mathrm{Al_2O_3} \quad (4)$$

SEM images of film F40 are shown in Figure 2B and C. The low magnification image shows that the thickness (≈28 μm) of the film is uniform, while some fibrous polymer network can be seen in the film at high magnification (Figure 2C). The SEM images of the other films with different mass loadings are displayed in Figure S8.

The mechanical properties of $Bi(IO_3)_3$/Al/PVDF films with different mass loading are shown in Figure 2D and Table 3. The addition of $Bi(IO_3)_3$ and Al nanoparticles decreased the tensile strength of the PVDF film from 36.6 MPa at 0 wt% to 26.6 MPa at 62.9 wt%. This is to be expected, and is consistent with our previous results.[21] The Young's modulus increased from 152 to 517 MPa, with the mass loading increase from 0 to 62.9 wt %.[42–44] While the mechanical properties did degrade with the increasing of nano particle mass loading, the resultant films even with these high loadings were still flexible, crack-free, and could be easily handled without damage.

3.4.2. T-Jump/TOFMS of Films

For T-jump measurments $Bi(IO_3)_3$/Al/PVDF films (Film of F40 listed in Table 4) were directly deposited on the Pt-wire by our electrospray method as shown in Figure S2B. Upon

DOI: 10.1002/adem.201500532

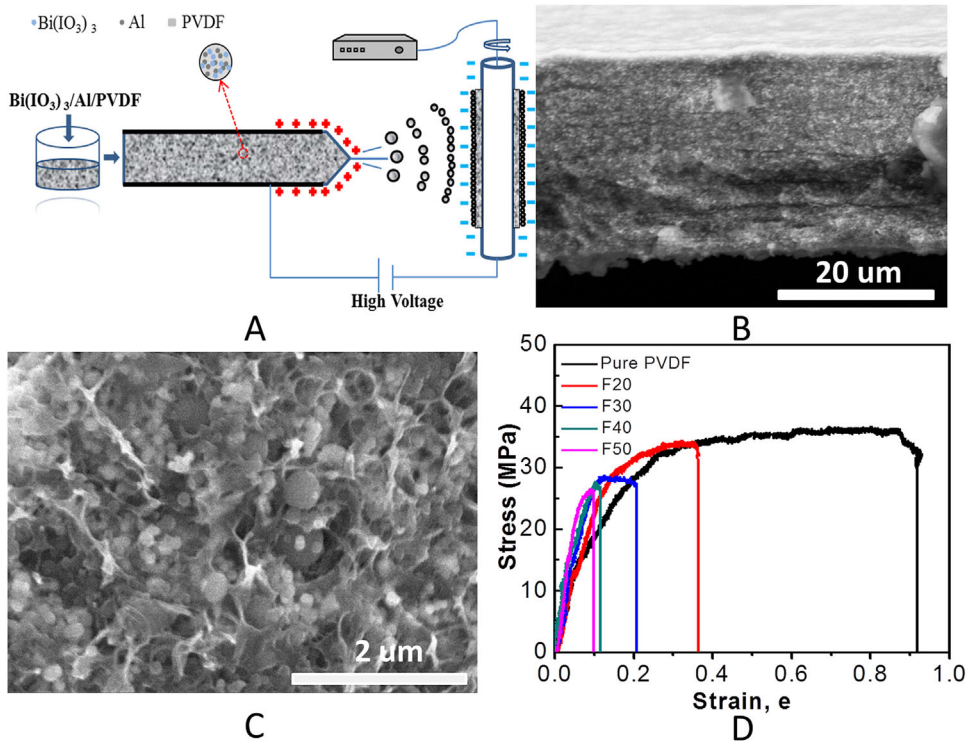

Fig. 2. (A) Schematic illustration of film deposition system; (B) cross-section of film F40; (C) close-up of film cross-section F40; (D) stress–strain curves of films with different mass loadings.

ignition (Figure S9), H_2^+, Bi^+, and I_2^+ are observed consistent with Equation 3 and 4. The ignition temperature of $Bi(IO_3)_3$/Al/PVDF films in vacuum, argon and air are 850, 530, and 520 °C, respectively, with the combustion in argon and air much more vigorous than that in vacuum as shown in Figure S6B, C, and D. We can conclude based on these results and similar prior results,[45,46] that the thermite initiates through oxygen generated by the iodate, rather than from any fluorine initiated reaction. The decrease in ignition temperature in a pressurized atmosphere is attributed to the higher local concentration of reactive gaseous species near the Al-NPs relative to vacuum. The fact that there was little difference between air or argon implies that the local generation of oxygen from the iodate far exceeds the available oxygen flux to the aluminum from the ambient oxygen in air. This is consistent with recent work of ours in high-pressure O_2 which showed that increased oxygen pressure can lower ignition temperature for weak thermites but had no effect on strong thermites.[47]

Table 3. Young's modulus of films at different mass loading

Film	Film		Young's modulus [MPa]	Particle mass loading in film [%]
	Equation 3	Equation 4		
PVDF	Pure PVDF		152	0
F20	80%	20%	301	40.6
F30	70%	30%	344	48.0
F40	60%	40%	363	55.5
F50	50%	50%	517	62.9

3.4.3. Combustion Properties of Films

Compared with $Bi(IO_3)_3$/Al, the reaction of $Bi(IO_3)_3$/Al/PVDF film is more violent presumably because of high heat released from reaction between Al and PVDF leading to AlF_3. Propagation velocity was evaluated for $3 \times 0.5\,cm^2$ $Bi(IO_3)_3$/Al/PVDF films run in triplicate to obtain an average propagation velocity in both argon and air as shown in Figure 3. As shown in Figure 3A, the propagation velocity of $Bi(IO_3)_3$/Al/PVDF decreased with higher iodate mass fraction (i.e., Equation 4) in both air and argon. In these films, PVDF acts as binder, as well as oxidizer. As shown in Figure 3B, the related peaks of AlF_3, Al_2O_3, Bi, I_2, and C are observed in the XRD pattern of $Bi(IO_3)_3$/Al/PVDF film, combustion products in argon. Considering the main decomposition product of PVDF (reaction products in the T-jump result (Figure S9), and the XRD pattern (Figure 3B), in argon, we postulate the reaction between aluminum and PVDF proceeds through Equation 3, and that reactions between $Bi(IO_3)_3$ and Al can be described as Equation 4, consistent with our previous study.[45] The heats of reaction for Equation 3 and 4 are, −947.7 and −712.3 kJ (mol of aluminum)$^{-1}$, respectively. The formation energy of PVDF was calculated from the combustion heat obtained from Brandup et al.,[48] and the formation energy of $Bi(IO_3)_3$ was calculated based on the DSC measurement (the formation

DOI: 10.1002/adem.201500532

Table 4. Film formulations with different mass loadings and equivalence ratio, φ

No.	Films	Al [mg]	$Bi(IO_3)_3$ [mg]	PVDF [mg]	φ	Computed enthalpy per unit volume of film (in air) [kJ cm^{-3}]	Al and $Bi(IO_3)_3$ Mass loading in films [%]
1	F40-0.50Bi	107.9	70.6	200	1.22	39.2	47.2
2	F40-1.0	107.9	141.2	200	1	36.1	55.5
3	F40-1.5Bi	107.9	211.8	200	0.85	27.8	61.5
4	F40-0.5P	107.9	141.2	100	1.47	38.7	71.3
5	F40-1.5P	107.9	141.2	300	0.76	27.1	45.4

Note: Active aluminum content is 81%. In F40-0.5Bi film and F40-1.5Bi film, the amount of $Bi(IO_3)_3$ was changed to adjust φ; In F40-0.5P film and F40-1.5P film, the amount of PVDF was changed to adjust φ.φ is calculated by Equation 6 displayed below.

$$\varphi = \frac{\text{Fuel}_{ACT}}{\text{Fuel}_{STO}} \quad (6)$$

Where, Fuel_{ACT} is the actual active aluminum content. Fuel_{STO} is calculated from the masses of $Bi(IO_3)_3$ and PVDF according to Equation 3 and 4. The detailed calculation of φ is displayed in the supporting materials.

energy of Bi_2O_3 obtained from Binnewies[41]). Thus leads to concluding that the heat of combustion between Al and PVDF is considerably higher than that between nanothermite,[28] supporting the result that the heat released from Equation 3 is much higher than that of Equation 4 and consistent with the higher propagation velocity.

In comparison to argon, the propagation velocity in air was more sensitive to iodate loading, since with the addition of higher contributions of Equation 4, less hydrogen (and carbon) is produced from Equation 3 to react with oxygen in air. The overall reaction in air can be described with Equation 5, whose heat of combustion is −2 556 kJ (mol of aluminum)$^{-1}$, is more than double that of Equation 3. Direct evidence for this point is that the carbon peaks in the XRD under air oxidation is small, while the Al_2O_3 peaks in the residue is significantly higher than AlF_3 suggesting that available oxygen in air reacted with Al to a significant extent (Figure 3B). Visually, the combustion of films in air was much more violent than that in argon (Figure S10), consistent with results from the T-jump and combustion evaluations above.

$$3(CH_2 - CF_2)_n + 2n\text{Al} + 7.5n\text{O}_2 - 6n\text{CO}_2 + 2n\text{AlF}_3 + 3n\text{H}_2\text{O} \quad (5)$$

To further evaluate how mass loading of solid particles, and fuel/oxidizer ratio impact the combustion properties the mass loading of $Bi(IO_3)_3$ and PVDF were varied as summarized in Table 4.

For evaluation of reaction propagation, the equivalence ratio, φ, was varied through changes in either $Bi(IO_3)_3$ or PVDF as displayed in Table 4. Not surprisingly, and consistent with Figure 3A, propagation in air is faster than in argon even under fuel lean conditions. In Figure 4, the propagation velocity is presented for the films listed in Table 4 as a function of equivalence ratio, φ. With the exception of $\varphi = 0.85$, propagation velocity in argon increases with equivalence ratio, and is in general also true in air, however velocity decreases above $\varphi = 1.22$. This result of a minimum at $\varphi = 0.85$, probably results from the fact that changing equivalence ratio in this system actually involves changing more than one variable, in this case both the PVDF and iodate. The rise in propagation velocity with increasing φ indicates that having excess aluminum leads to faster overall reaction and implies that the oxidation of aluminum in the early part of the reaction (i.e., to generate the heat to drive the propagation) must be slow and presumably why adding air at least initially till $\varphi > 1.22$ increases reaction velocity. However as discussed for the minimum, the location of the maximum is also a manifestation of the complex nature of the mixture, and the two parallel global Equation 4 and 5.

To explain this further, we consider an alternative metric, the reaction exothermicity per unit volume of film. From the experimental mass loadings, and the known material densities[21,40] as well as the heats of formation, we can compute the expected heat release per unit volume, which is also presented in Table 4. Propagation should be faster if the energy

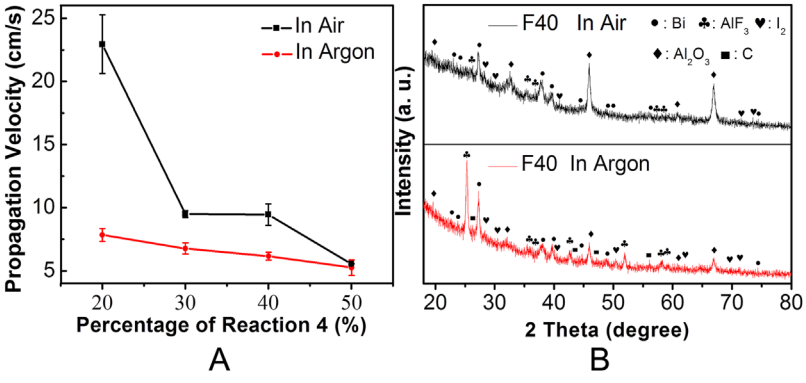

Fig. 3. (A) Propagation velocity of films with different mass loadings in air and argon; (B) XRD patterns of combustion products of $Bi(IO_3)_3$/Al/PVDF film in air and argon. Note: The equivalence ratio of all films in this figure equals unity.

FULL PAPER

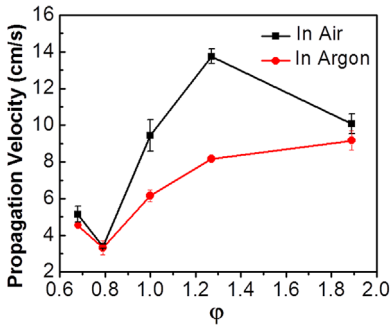

Fig. 4. Propagation velocity of films with different φ, in argon and air.

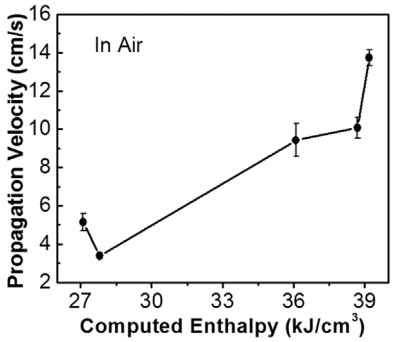

Fig. 5. Relationship between propagation velocity of films in air and corresponding to enthalpy of reaction from Equation 4 and 5. (Assuming air is not mass transfer constrained).

density is higher at a fixed effective thermal diffusivity, and the global reaction activation energy is relatively constant. Presented in this way, reaction velocity which mostly increases with equivalence ratio (under rich conditions) scales with reaction exothermicity shown in Figure 5. This is because the heat release from Equation 5, is larger than Equation 4 (i.e., the iodate reaction is less energetic). From a practical point of view, however, it is the argon case that is the more relevant since the air case is material length scale (O_2 mass transfer rate) dependent. A thicker film will have a smaller air reaction component to contribute.

4. Conclusions

In this study, a multifunctional reactive material ($Bi(IO_3)_3$/Al thermite) was developed with biocidal combustion products, which can remain active for an extended period of time well past the thermal and pressure pulse for bioagents. Films consisted of synthesized metal iodate, nanoaluminum and PVDF which were deposited using an electrospray method, and found to have good mechanical characteristics at high particulate loadings. T-jump/TOFMS and combustion test results demonstrate that $Bi(IO_3)_3$ containing films are highly energetic, which release elemental iodine, suggesting that $Bi(IO_3)_3$/Al/PVDF film can be a candidate as a biocidal energetic.

Article first published online: xxxx
Manuscript Revised: March 7, 2016
Manuscript Received: October 22, 2015

[1] J. A. Higgins, M. S. Ibrahim, F. K. Knauert, G. V. Ludwig, T. M. Kijek, J. W. Ezzell, B. C. Courtney, E. A. Henchal, *Ann. N. Y. Acad. Sci.* **1999**, *894*, 130.
[2] C. Farley, M. Pantoya, *J. Therm. Anal. Calorim.* **2010**, *102*, 609.
[3] M. Leitenberg, *Meeting the Challenges of Bioterrorism: Assessing the Threat and Designing Biodefense Strategies*, The Strategic Studies Institute, Zurich, Switzerland **2005**.
[4] S. Yan, G. Jian, M. R. Zachariah, *ACS Appl. Mater. Interfaces* **2012**, *4*, 6432.
[5] H. Wang, G. Jian, G. C. Egan, M. R. Zachariah, *Combust. Flame* **2014**, *161*, 2203.
[6] C. Rossi, A. Estève, P. Vashishta, *J. Phys. Chem. Solids* **2010**, *71*, 57.
[7] N. H. Yen, L. Y. Wang, *Propellants Explos. Pyrotech.* **2012**, *37*, 143.
[8] M. A. Ilyushin, I. V. Tselinsky, I. V. Shugalei, *Cent. Eur. J. Energ. Mater.* **2012**, *9*, 293.
[9] S. Zhang, M. Schoenitz, E. L. Dreizin, *J. Phys. Chem. C* **2010**, *114*, 19653.
[10] A. Abraham, S. Zhang, Y. Aly, M. Schoenitz, E. L. Dreizin, *Adv. Eng. Mater.* **2014**, *16*, 909.
[11] Y. Aly, S. Zhang, M. Schoenitz, V. K. Hoffmann, E. L. Dreizin, M. Yermakov, R. Indugula, S. A. Grinshpun, *Combust. Flame* **2014**, *161*, 303.
[12] S. A. Grinshpun, A. Adhikari, M. Yermakov, T. Reponen, E. Dreizin, M. Schoenitz, V. Hoffmann, S. Zhang, *Environ. Sci. Technol.* **2012**, *46*, 7334.
[13] B. R. Clark, M. L. Pantoya, *Phys. Chem. Chem. Phys.* **2010**, *12*, 12653.
[14] G. Jian, S. Chowdhury, J. Feng, M. R. Zachariah, *U. S. Natl. Combust. Meet., 8th*, Park City, UT **2013**.
[15] K. T. Sullivan, N. W. Piekiel, S. Chowdhury, C. Wu, M. R. Zachariah, C. E. Johnson, *Combust. Sci. Technol.* **2011**, *183*, 285.
[16] K. T. Sullivan, C. Wu, N. W. Piekiel, K. Gaskell, M. R. Zachariah, *Combust. Flame*, **2013**, *160*, 438.
[17] C. E. Johnson, K. T. Higa, *Mater. Res. Soc. Symp. Proc.* **2013**, *1521*.
[18] A. D. Russell, *J. Antimicrob. Chemother.* **2003**, *52*, 750.
[19] A. D. Russell, I. Ahonkhai, D. T. Rogers, *J. Appl. Bacteriol.* **1979**, *46*, 207.
[20] H. Wang, G. Jian, W. Zhou, J. B. Delisio, V. T. Lee, M. R. Zachariah, *ACS Appl. Mater. Interfaces* **2015**, *7*, 17363.
[21] C. Huang, G. Jian, J. B. Delisio, H. Wang, M. R. Zachariah, *Adv. Eng. Mater.* **2015**, *17*, 95.
[22] A. Zenin, *J. Propuls. Power* **1995**, *11*, 752.

DOI: 10.1002/adem.201500532

[23] W. Zheng, J. Wang, X. Ren, L. Zhang, Y. Zhou, *Propellants Explos. Pyrotech.* **2007**, *32*, 520.
[24] K. Meeks, M. L. Pantoya, C. Apblett, *Combust. Flame* **2014**, *161*, 1117.
[25] L. Galfetti, L. T. De Luca, F. Severini, L. Meda, G. Marra, M. Marchetti, M. Regi, S. Bellucci, *J. Phys. Condens. Matter.* **2006**, *18*, S1991.
[26] L. Meda, G. Marra, L. Galfetti, S. Inchingalo, F. Severini, L. De Luca, *Compos. Sci. Technol.* **2005**, *65*, 769.
[27] R. H. B. Bouma, D. Meuken, R. Verbeek, M. M. Pacheco, L. Katgerman, *Propellants Explos. Pyrotech.* **2007**, *32*, 447.
[28] K. W. Watson, M. L. Pantoya, V. I. Levitas, *Combust. Flame* **2008**, *155*, 619.
[29] Y. Yang, S. Wang, Z. Sun, D. D. Dlott, *J. Appl. Phys.* **2004**, *95*, 3667.
[30] X. Li, P. Guerieri, W. Zhou, C. Huang, M. R. Zachariah, *ACS Appl. Mater. Interfaces* **2015**, *7*, 9103.
[31] G. Jian, J. Feng, R. J. Jacob, G. C. Egan, M. R. Zachariah, *Angew. Chemie Int. Ed.* **2013**, *52*, 9743.
[32] L. Zhou, N. Piekiel, S. Chowdhury, M. R. Zachariah, *Rapid Commun. Mass Spectrom.* **2009**, *23*, 194.
[33] G. Jian, N. W. Piekiel, M. R. Zachariah, *J. Phys. Chem. C* **2012**, *116*, 26881.
[34] G. Jian, L. Zhou, N. W. Piekiel, M. R. Zachariah, *ChemPhysChem* **2014**, *15*, 1666.
[35] L. Zhou, N. Piekiel, S. Chowdhury, M. R. Zachariah, *J. Phys. Chem. C* **2010**, *114*, 14269.
[36] A. L. Gershon, D. P. Cole, A. K. Kota, H. A. Bruck, *J. Mater. Sci.* **2010**, *45*, 6353.
[37] A. L. Gershon, A. K. Kota, H. A. Bruck, *J. Compos. Mater.* **2009**, *43*, 2587.
[38] K. Sullivan, M. Zachariah, *J. Propuls. Power* **2010**, *26*, 467.
[39] G. Jian, L. Liu, M. R. Zachariah, *Adv. Funct. Mater.* **2013**, *23*, 1341.
[40] B. Bentria, D. Benbertal, M. B. Beucher, R. Masse, A. Mosset, *J. Chem. Crystallogr.* **2003**, *33*, 867.
[41] M. Binnewies, E. Mike, *Thermochemical Data of Elements and Compounds*, Wiley VCH Verlag GmbH, Weinheim, New York, United State **2002**.
[42] T. Sekitani, Y. Noguchi, K. Hata, T. Fukushima, T. Aida, T. Someya, *Science* **2008**, *321*, 1468.
[43] D. Wu, X. Wang, Y. Song, R. Jin, *J. Appl. Polym. Sci.* **2004**, *92*, 2714.
[44] K. Yang, Q. Yang, G. Li, Y. Sun, D. Feng, *Mater. Lett.* **2006**, *60*, 805.
[45] J. B. Delisio, C. Huang, G. Jian, M. R. Zachariah, G. Young, AIAA Sci Tech *52nd Aerospace Sciences Meeting, National Harbor*, Maryland **2014**.
[46] W. Zhou, J. B. DeLisio, X. Li, L. Liu, M. R. Zachariah, *J. Mater. Chem. A* **2015**, *3*, 11838.
[47] W. Zhou, J. B. DeLisio, X. Wang, G. C. Egan, M. R. Zachariah, *J. Appl. Phys.* **2015**, *118*, 114303.
[48] J. Brandup, E. Immergut, E. Grulke, *Polymer Handbook*, John Wiley & Sons, Inc, NY, USA **1999**.